ADVANCES IN ATMOSPHERIC SCIENCES, VOL. 22, NO. 1, 2005, 1–20

Seasonal Variability of the Yellow Sea/East China Sea Surface Fluxes and Thermohaline Structure

Peter CHU*[1], CHEN Yuchun[2] (陈玉春), and Akira KUNINAKA[1]

[1]*Naval Ocean Analysis and Prediction Laboratory,*

Department of Oceanography Naval Postgraduate School, Monterey, California

[2]*Institute of Cold and Arid Environment and Engineering, Chinese Academy of Sciences, Lanzhou*

(Received 27 November 2003; revised 26 April 2004)

ABSTRACT

We use the U.S. Navy's Master Oceanographic Observation Data Set (MOODS) for the Yellow Sea/East China Sea (YES) to investigate the climatological water mass features and the seasonal and non-seasonal variabilities of the thermohaline structure, and use the Comprehensive Ocean-Atmosphere Data Set (COADS) from 1945 to 1989 to investigate the linkage between the fluxes (momentum, heat, and moisture) across the air-ocean interface and the formation of the water mass features. After examining the major current systems and considering the local bathymetry and water mass properties, we divide YES into five regions: East China Sea (ECS) shelf, Yellow Sea (YS) Basin, Cheju bifurcation (CB) zone, Taiwan Warm Current (TWC) region, Kuroshio Current (KC) region. The long term mean surface heat balance corresponds to a heat loss of 30 W m^{-2} in the ESC and CB regions, a heat loss of 65 W m^{-2} in the KC and TWC regions, and a heat gain of 15 W m^{-2} in the YS region. The surface freshwater balance is defined by precipitation minus evaporation. The annual water loss from the surface for the five subareas ranges from 1.8 to 4 cm $month^{-1}$. The fresh water loss from the surface should be compensated for from the river run-off. The entire water column of the shelf region (ECS, YS, and CB) undergoes an evident seasonal thermal cycle with maximum values of temperature during summer and maximum mixed layer depths during winter. However, only the surface waters of the TWC and KC regions exhibit a seasonal thermal cycle. We also found two different relations between surface salinity and the Yangtze River run-off, namely, out-of-phase in the East China Sea shelf and in-phase in the Yellow Sea. This may confirm an earlier study that the summer fresh water discharge from the Yangtze River forms a relatively shallow, low salinity plume-like structure extending offshore on average towards the northeast.

Key words: Yellow Sea, East China Sea, surface net heat flux, fresh water flux, seasonal variability, thermohaline structure

1. Introduction

The combined Yellow Sea and East China Sea (called YES) covers roughly 1 250 000 km^2 and is one of the most developed continental shelf areas in the world (Yanagi and Takahashi, 1993). While the Yellow Sea (YS) covers a relatively large area, it is quite shallow reaching a maximum depth of about 140 m (Fig. 1). The water depth over most of the area is less than 50 m. The deepest water is confined to a north-south oriented trench which runs from the northern boundary south to the 100 m isobath where it fans out onto the continental shelf break. The bathymetric gradients are very small. Such a broad and shallow continental shelf sea suggests that the water column will be readily affected by seasonally varying atmospheric conditions such as heating, cooling, and wind stress. Therefore, the seasonal variation of the water masses is remarkably large. Another feature of the depth distribution is the east/west asymmetry. Extensive shoals (< 20 m) are located in the western Yellow Sea along the Chinese coast but are not generally found off the South Korean coastal regions. Also, the 50 m isobath is located more than 100 km from the Chinese coast, but only about 50 km from the South Korean coast. This asymmetry in bottom depth is important in controlling the mixed layer depth (Chu et al., 1997b).

*E-mail: pcchu@nps.navy.mil

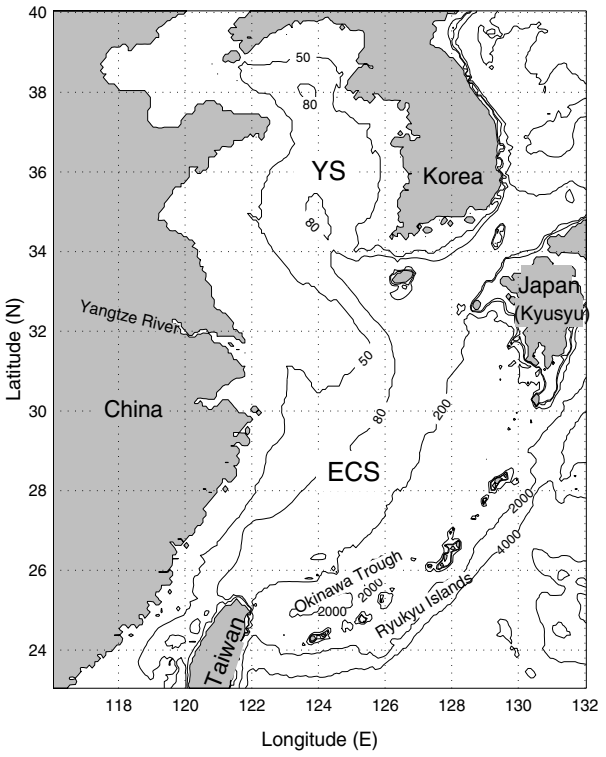

Fig. 1. Topography and isobaths of the East China Sea and the Yellow Sea.

The East China Sea (ECS) is located south of the YS to the north of Taiwan (Fig. 1). The ECS is usually defined as reaching from the northern end of the Taiwan Strait to the southern end of Kyusyu where it adjoins the YS along a line from Kyushu to Shanghai (the mouth of the Yangtze River). With the exception of the Okinawa Trough west of the Ryukyu Islands, which reaches 2 700 m depth, the ECS is part of the continental shelf. The hydrographic character of the water masses in YES depends on the bathymetry, the Kuroshio Current, the atmospheric forcing (monsoon winds, heat and moisture fluxes), and the degree of mixing of fresh water originating from Asian river runoff with the intrusion of Kuroshio waters (Tomczak and Godfrey, 1994).

To examine the seasonal variability of the water mass and circulation, we use the U.S. Navy's Master Oceanographic Observation Data Set (MOODS) to investigate the climatological features and the seasonal and non-seasonal variability of the thermohaline structure, and use the Comprehensive Ocean-Atmosphere Data Set (COADS) from 1945 to 1989 to investigate the linkage between the fluxes (momentum, heat, and moisture) across the air-ocean interface and the formation of the water mass features.

2. YES Oceanography and subdivision

2.1 *Water masses*

Earlier studies (e.g., Liu et al., 1992; Su and Weng, 1994; Chen et al., 1995) have shown that a complex water mass structure exists in YES based on temperature and salinity features. The water in the shallow parts of YES is affected greatly by the atmospheric and geographic conditions, and therefore it does not have the homogeneity as in the open ocean. Su and Weng (1994) proposed a concept of modified water mass holding similar physical and chemical characteristics and occupying a certain space.

Based on temperature data observed in 1978–1980, Su and Weng (1994) identified the following water masses using a successive clustering method on temperature observations: Kuroshio Surface Water (KSW), East China Sea Mixed Water (ECSMW), East China Sea Deep Water (ECSDW), Yellow Sea and East China Sea Mixed Water (YEMW), Yellow Sea Mixed Water (YSMW), Yellow Sea Bottom Cold Water (YSCW), Yellow Sea Near-shore Water (YSNW), and Continental Shelf Diluted Water (CSDW).

Since salinity is a more conserved quantity in the YES than temperature (Su and Weng, 1994), the water masses are classified into three systems based on their salinity features: (1) the ECS water system (or the open water system), including KSW, ECSMW, ECSDW, and YEMW (in May only) and originating from the Kuroshio Water Mass, (2) the YS water system (or the local water system), including YSMW, YSCW, YEMW, and (3) the coastal water system, including CSDW and YSNW.

Since the ECS water system is an open water system, horizontal advection, especially the meandering of the Kuroshio Current, should be an important factor in its variability. In contrast, the YS water system is a local system. The local atmospheric forcing should be responsible for its variability. In fact, the central region of the YS stands out due to its cold bottom water, which is YSCW. During summer, strong surface warming generates the sharpest thermocline on the top of the YSCW in the region. During winter, this water mass provides a significant buffer preventing central YS water temperatures from reaching the near-freezing temperatures that the near-shore regions experience (Chu et al., 1997a, b).

2.2 *Subdivision*

YS and ECS are separated at 32°N. Water masses and current systems on the shelf (depth less than 80 m) differ from those on the slope (80–200 m) and deeper

(depth greater than 200 m). Considering the bottom topography effect and current systems, YES is divided into five subregions (Fig. 2): (1) the ECS shelf with the eastern boundary at the 80 m bathymetry contour line and the northern boundary at 32°N, representing the coastal current system; (2) the YS shelf with the northern boundary at 38°30′N, the southern boundary at 32°N, the western boundary at 122°E in the mouth of the Gulf of Bohai and the Chinese coast, and the eastern boundary at the Korean coast and the 80 m depth contour line, representing the YS gyre system; (3) the Cheju bifurcation (CB) area with the northern and western boundaries at the 80 m contour, the eastern boundary at 127°15′E, and the southern boundary at 32°N, representing the Taiwan Warm Curent (TWC) branching into the Tsushima current and Yellow Sea Warm Current; (4) the TWC area bounded by the 80 m and 200 m bathymetric contours, and 32°N latitude, representing the TWC system; and (5) the Kuroshio area bounded by the 200 m and 4000 m contours, and 32°N latitude, representing the KC system.

3. Seasonal variation of the atmospheric forcing

3.1 *General description*

The Asian monsoon strongly affects the thermal structure of YES. During the winter monsoon season, a very cold northwest wind blows over the ECS/YS as a result of the Siberian High Pressure System. The Jet Stream is positioned to the south of the YS and the Polar Front to the north of the Philippines. By late April, the Polar Front has moved northward toward Korea with warm, moist air following behind. Numerous frontally-generated events occur making late April and May highly variable in terms of wind speeds and cloud amount. During this period storms originating in Mongolia may cause strong, warm westerlies carrying yellow desert sand (termed the "Yellow Wind"). By late May and early June, the summer surface atmospheric low pressure system begins to form over Asia. Initially this low pressure system is centered north of the Yellow Sea producing westerly winds. In late June, this low begins to migrate to the west setting up the southwest monsoon that dominates the summer months. The winds remain variable through June until strengthening of the Manchurian Low pressure system occurs. The Jet Stream migrates just south of Korea, and the Polar Front is just south of Kyushu and Shikoku. Despite the very active weather systems, the mean surface wind speed over the central Yellow Sea in summer is between 3 and 4 m s^{-1}, which is weaker than in winter. June also marks, historically, a jump in precipitation associated with warm, moist air south of the Polar Front (Watts, 1969). Occasionally the Okhotsk High blocks the northerly progression of the Polar Front. By July, however, high pressure (the Bonin High) to the south and the low pressure over Manchuria produce southerly winds carrying warm, moist air over YES.

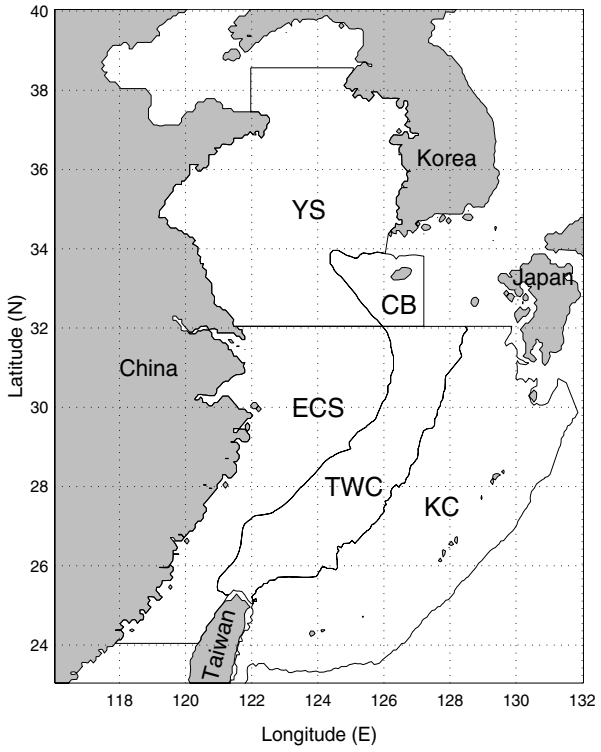

Fig. 2. Subdivisions of ECS/YS.

The summer monthly mean surface air temperature (SAT) is usually 1.5–2°C warmer than the mean sea surface temperature (SST) (Van Loon, 1984). The warmer air causes a downward heat flux at the air-ocean interface. This heat flux plus the strong downward net radiation stabilizes the upper layer of the water and causes the surface mixed layer to shoal, creating a multi-layer structure. Below the thermocline in the YS, there is a cold water mass, commonly referred to as Yellow Sea Bottom Cold Water (YSCW) that remains unchanged and nearly motionless throughout the summer (Li and Yuan, 1992). October is the beginning of the transition back to the winter conditions. The southerly winds weaken, letting the sea surface slope reestablish the winter pattern. The YS SST steadily decreases from 12°C in October to 4°C in January (Chu et al., 1997a).

3.2 *Surface climatology*

Here, we present a climatological description of the atmospheric conditions over YES and their effect in

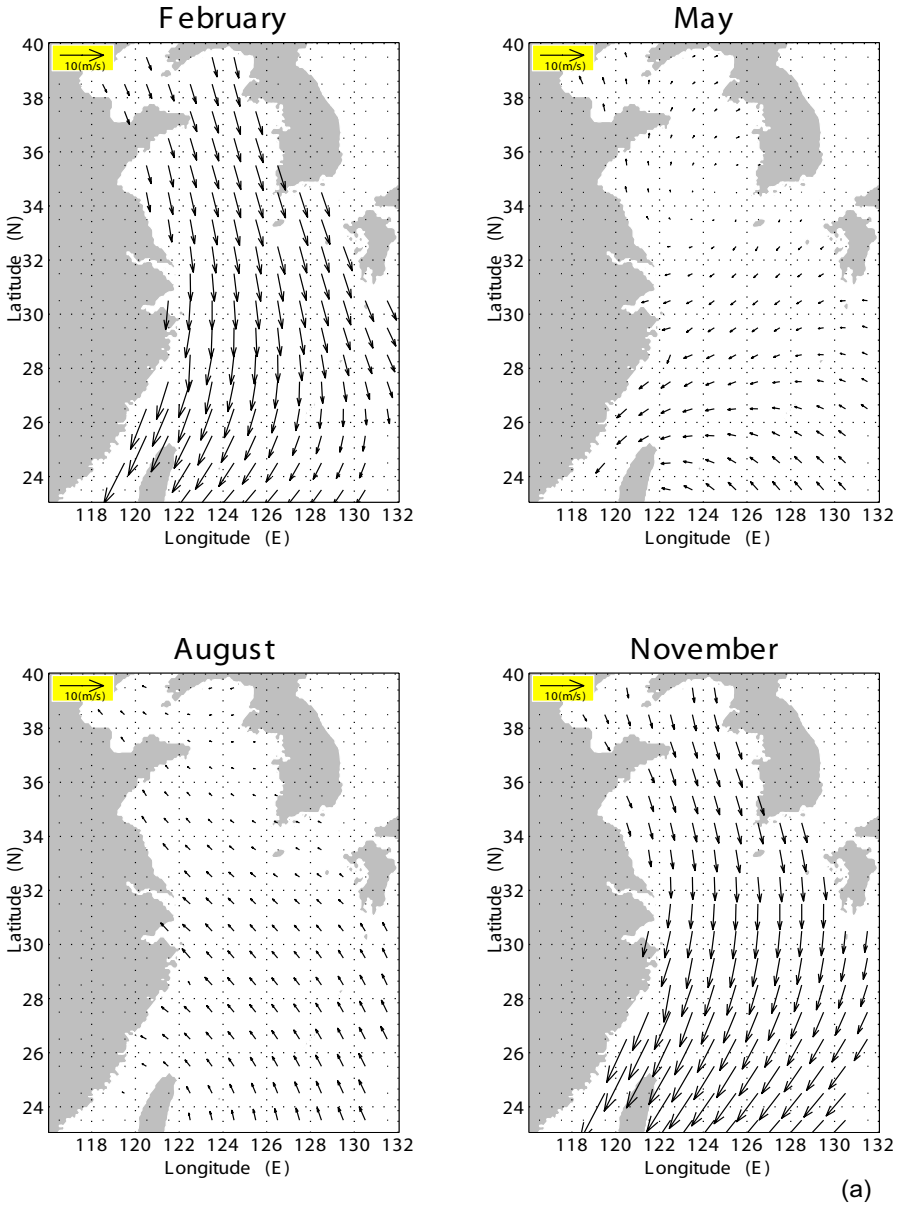

Fig. 3. (a) Average surface winds for February, May, August, and November from COADS. (b) Average surface air temperature (°C) for February, May, August, and November from COADS. (c) Average surface relative humidity (%) for February, May, August, and November from COADS.

terms of heat exchange and storage, derived from the $1° \times 1°$ COADS data (1945–1989). The climatological monthly mean values of wind speed, temperature and relative humidity are shown in Fig. 3a–c for the months of February, May, August, and November, which may be regarded as representative patterns for each season.

The main characteristic of the COADS wind data (Fig. 3a) is the seasonal variation of the monsoon winds. In winter, strong north to northwest winds prevail in the northern YES and north to northeast winds prevail in the southern YES. In summer, weak southeast winds prevail. May is the summer monsoon transition period. The surface winds over the YS are very weak (mean monthly wind speed less than $3\ \mathrm{m\ s^{-1}}$) both in summer and during the summer monsoon transition period.

The SAT exhibits seasonal fluctuations of about 22°C in the YS and about 10°C in the ECS, averaging about 17°C over the entire domain (Fig. 3b). A nearly latitudinal gradient prevails in all seasons with the

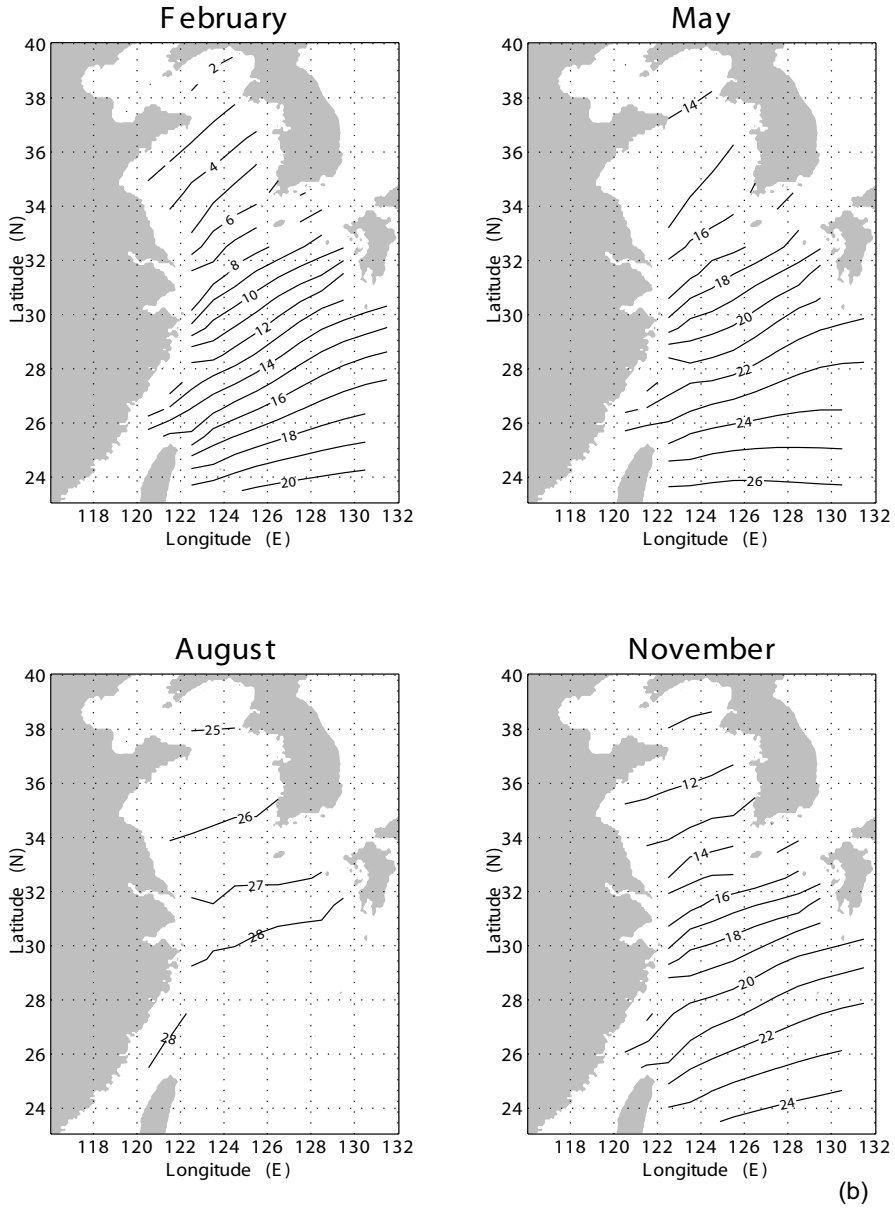

Fig. 3. (Continued).

maximum south-to-north mean SAT difference of 18°C in February and the minimum SAT difference of 3°C in August. The SAT is uniformly warm (mean SAT around 28°C) in the ECS during summer (August).

Surface relative humidity (Fig. 3c) is generally higher in the summer season, mainly as a consequence of the southeast summer monsoon bringing moist air from the Tropics. The summer field is relatively homogeneous (83%) in the ECS, whereas a significant latitudinal gradient exists in the other seasons. A relative humidity minimum (maximum) is present in all seasons near Kyushu Island (Chinese coast), which may lead to maximum (minimum) evaporation there.

3.3 *Surface fluxes*

Fluxes across the air-ocean interface drive oceanic processes. Recent studies (Chu et al., 1998) show that the Haney type sea surface boundary condition (Haney, 1971) is not valid for regional seas. For the YES modeling, it is necessary to use all the fluxes (Chu et al. 2001).

3.3.1 *Net heat flux*

Net surface heat flux ($Q_{\rm net}$) is computed by

$$Q_{\rm net} = R_{\rm s} - (R_{\rm l} + Q_{\rm l} + Q_{\rm s}) \qquad (1)$$

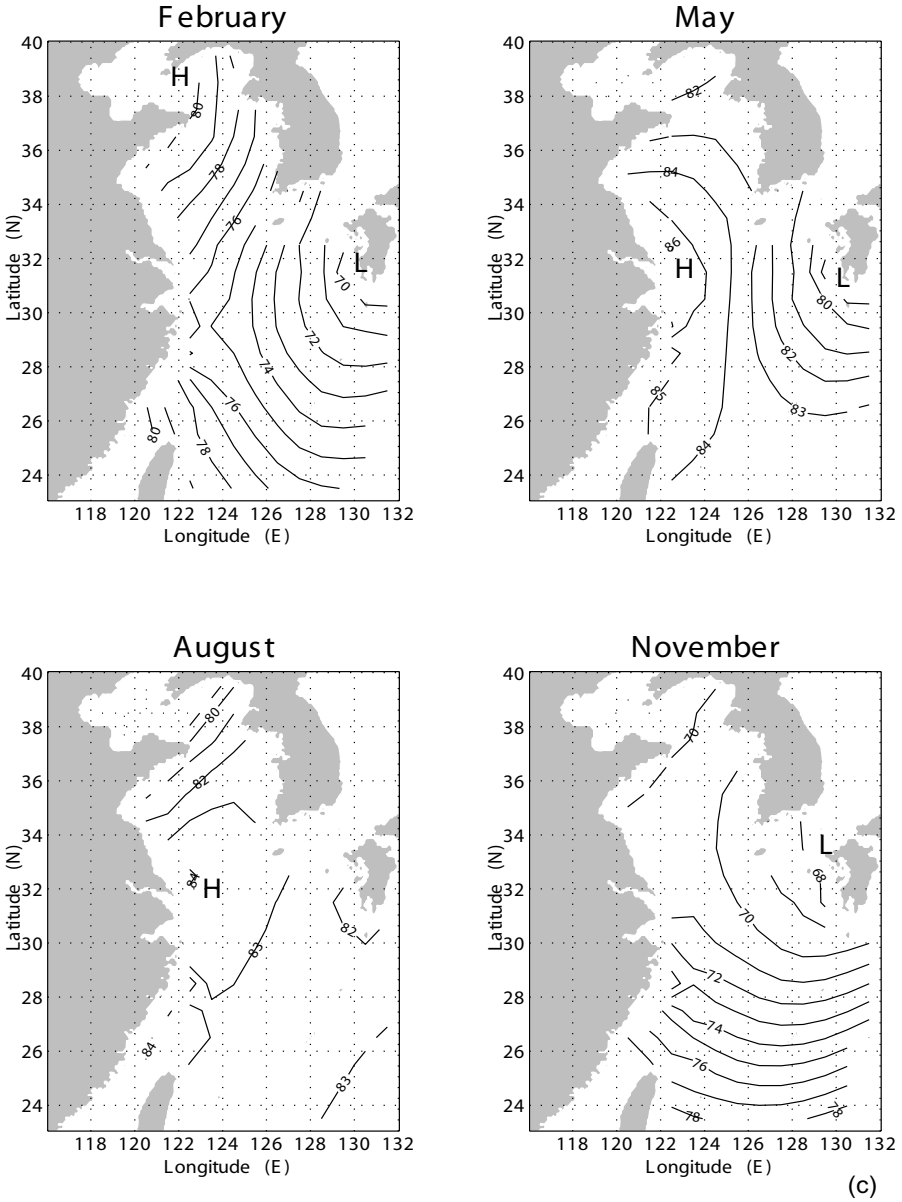

Fig. 3. (Continued).

where R_s is the net downward shortwave radiation, R_l the net upward longwave radiation, Q_l the sensible heat flux, and Q_s the latent heat flux. Positive (negative) values of Q_{net} indicate net heat gain (loss) of the ocean at the surface. The fluxes (R_s, R_l, Q_l, Q_s) are directly obtained from the COADS dataset. The summer field is relatively homogeneous (120–160 W m^{-2}) in the whole YES, whereas a significant horizontal gradient with a minimum center near Kyushu Island exists in the other seasons (Fig. 4). The ocean surface near Kyushu Island belonging to the KC and TWC sub-regions has a maximum heat loss of 280 W m^{-2} in the winter (November to February), and a minimum heat gain of 80 W m^{-2} in the spring. This long term net surface heat loss will be compensated for by the advection of warm tropical waters by KC and TWC. Besides, there is an increase of net surface heat gain (flux downward) toward the Chinese coast in all seasons, which might be caused by less evaporation there.

The annual mean heat budget is positive in the YS region (15 W m^{-2}) and negative elsewhere: around –30 W m^{-2} in the ECS and CB regions, and –65 W m^{-2} in the KC and TWC regions (Tables 1–5). These values consist with recent calculations (Hirose

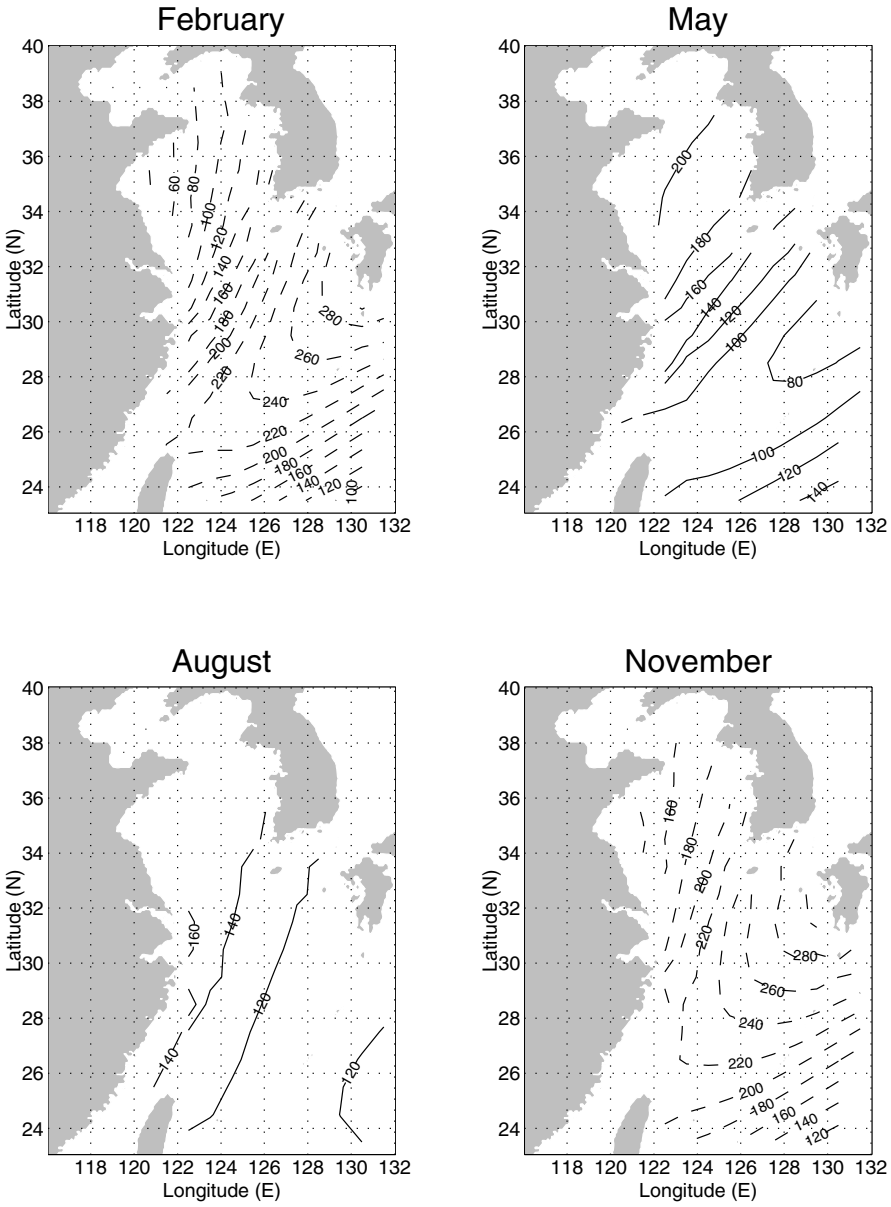

Fig. 4. Average net surface heat flux (W m^{-2}) for February, May, August, and November from COADS. Solid (dashed) lines indicate positive (negative) values.

et al., 1999). A low annual mean latent heat flux in the YS region causes the positive annual heat budget. Sensible heat flux is nearly zero in summer, which implies SST is close to SAT. The ratio between sensible and latent heat fluxes (defined as the Bowen ratio) is listed in the seventh column of these tables. The Bowen ratio has the following features: (1) a value less than one for any month for all five sub-areas, indicating larger latentheat flux than the sensible heat flux, (2) a seasonal variation with relatively large values (0.33–0.67) in winter and near zero values in summer, and (3) larger annual variation in the shallow water regions (YS, CB) than in the relatively deep water regions (KC and TWC).

The monthly variation of net surface heat flux (Fig. 5) is nearly sinusoidal and quite similar among the five sub-areas. The YS region leads the rest of the sub-areas by half to one month: $Q_{\rm net}$ becomes positive in mid-February in the YS region, in early March in the ECS and CB regions, and in late March in the KC and TWC regions. $Q_{\rm net}$ peaks in June in the YS region and in July in the rest of the sub-areas.

Table 1. Monthly surface heat flux components obtained from COADS data for the ECS shelf region.

Month	R_s (W m^{-2})	R_l (W m^{-2})	Q_s (W m^{-2})	Q_l (W m^{-2})	Q_{net} (W m^{-2})	Q_s/Q_l
Jan	93.6	78.6	78.3	191.4	–254.8	0.41
Feb	122.0	71.4	64.3	159.3	–173.0	0.40
Mar	165.0	62.4	35.0	116.8	–49.2	0.30
Apr	208.0	51.5	14.0	70.8	71.3	0.20
May	234.8	43.5	5.4	49.5	136.4	0.11
Jun	241.2	34.3	1.5	39.4	166.0	0.04
Jul	269.7	33.1	–2.8	43.7	195.7	-0.06
Aug	257.4	38.4	0.1	72.8	146.1	0.00
Sep	207.5	47.9	8.1	128.6	22.8	0.06
Oct	158.5	62.0	22.4	190.5	–116.6	0.12
Nov	110.5	70.0	43.8	205.5	–208.9	0.21
Dec	89.0	79.3	71.6	212.0	–274.2	0.34
Annual Mean	179.7	56.1	28.5	123.4	–28.2	0.23

Table 2. Monthly surface heat flux components obtained from COADS data for the YS region.

Month	R_s (W m^{-2})	R_l (W m^{-2})	Q_s (W m^{-2})	Q_l (W m^{-2})	Q_{net} (W m^{-2})	Q_s/Q_l
Jan	82.1	88.8	76.8	114.2	–197.7	0.67
Feb	117.6	79.1	53.3	78.7	–93.4	0.68
Mar	172.0	68.5	16.0	44.9	42.6	0.36
Apr	222.3	57.3	0.2	23.2	141.6	0.01
May	261.4	21.1	–1.0	13.6	197.7	–0.07
Jun	260.3	39.0	–1.7	14.4	208.6	–0.12
Jul	247.6	32.4	–2.6	15.8	202.0	–0.16
Aug	245.8	39.1	0.7	57.7	148.3	0.01
Sep	194.3	56.5	8.8	114.8	14.2	0.08
Oct	149.7	73.2	23.2	133.6	–80.3	0.17
Nov	99.7	84.6	48.2	137.6	–170.7	0.35
Dec	75.1	90.7	74.7	137.6	–228.0	0.54
Annual Mean	177.3	63.4	24.7	73.8	15.4	0.33

Table 3. Monthly surface heat flux components obtained from COADS data for the CB region.

Month	R_s (W m^{-2})	R_l (W m^{-2})	Q_s (W m^{-2})	Q_l (W m^{-2})	Q_{net} (W m^{-2})	Q_s/Q_l
Jan	81.4	88.8	95.7	172.5	–275.6	0.55
Feb	116.6	79.2	70.8	136.1	–169.4	0.52
Mar	166.5	70.1	32.6	94.4	–30.5	0.35
Apr	212.1	57.0	10.0	51.2	93.9	0.20
May	248.0	48.8	2.9	32.4	163.8	0.09
Jun	241.1	36.0	1.6	24.9	178.5	0.06
Jul	247.2	32.0	–1.3	26.6	189.8	–0.05
Aug	245.4	38.8	2.7	68.7	135.1	0.04
Sep	190.7	51.8	12.4	127.9	–1.3	0.10
Oct	150.4	71.2	29.5	180.6	–130.9	0.16
Nov	103.2	83.7	56.0	192.0	–228.5	0.29
Dec	77.8	91.5	90.3	198.5	–302.5	0.45
Annual Mean	173.4	62.4	33.6	108.8	–31.5	0.31

Table 4. Monthly surface heat flux components obtained from COADS data for the TWC region.

Month	R_s (W m^{-2})	R_l (W m^{-2})	Q_s (W m^{-2})	Q_l (W m^{-2})	Q_{net} (W m^{-2})	Q_s/Q_l
Jan	93.1	81.6	88.1	233.0	–309.7	0.38
Feb	120.5	74.4	74.3	207.1	–235.4	0.36
Mar	162.6	65.2	44.6	159.6	–106.8	0.28
Apr	206.1	53.7	20.3	104.2	27.9	0.19
May	230.2	44.4	9.9	77.5	98.3	0.13
Jun	238.0	34.6	4.2	57.2	142.1	0.07
Jul	269.9	34.5	–0.2	62.6	172.9	0.00
Aug	254.2	39.0	2.6	88.2	124.3	0.03
Sep	207.5	47.3	9.8	136.5	13.9	0.07
Oct	158.5	62.1	25.9	211.8	–141.3	0.12
Nov	110.9	70.4	47.4	235.6	–242.5	0.20
Dec	89.7	57.4	33.6	151.9	–64.5	0.18
Annual Mean	178.4	57.4	33.6	151.9	–64.5	0.18

Table 5. Monthly surface heat flux components obtained from COADS data for the KC region.

Month	R_s (W m^{-2})	R_l (W m^{-2})	Q_s (W m^{-2})	Q_l (W m^{-2})	Q_{net} (W m^{-2})	Q_s/Q_l
Jan	99.4	80.5	81.4	248.0	–310.5	0.33
Feb	126.9	73.8	68.9	221.7	–237.6	0.31
Mar	168.5	65.3	43.4	173.9	–114.2	0.25
Apr	211.8	53.7	20.0	118.7	19.5	0.17
May	233.8	44.1	10.5	92.0	87.2	0.11
Jun	243.3	25.1	4.6	67.9	135.7	0.07
Jul	272.9	26.3	1.3	77.3	157.9	0.02
Aug	253.4	39.2	3.3	95.2	115.7	0.03
Sep	213.8	45.6	8.6	130.2	29.4	0.07
Oct	163.3	58.6	24.2	210.0	–129.5	0.12
Nov	116.3	66.7	42.7	238.8	–232.0	0.18
Dec	95.3	78.3	67.6	256.7	–307.2	0.26
Annual Mean	183.2	56.4	31.4	160.9	–65.5	0.20

3.3.2 *Fresh water flux*

The surface fresh water flux is the difference between precipitation rate (P) and evaporation rate (E),

$$F = P - E \,. \tag{2}$$

Positive values of F indicate a net water mass gain of the ocean at the surface. The surface fresh water flux exhibits distinct winter and summer patterns (Fig. 6). The summer pattern is characterized by fresh water gain in the whole area, and a saddle-type distribution with two low centers, one in the east (less than 3 cm month^{-1} near Kyushu Island) and the other in the west (less than 1 cm month^{-1} near the Chinese coast). Centers of high fresh water flux are found in the north (more than 14 cm month^{-1} in northern YS) and in the south (8 cm month^{-1}). The winter pattern is characterized by fresh water loss in the whole area with a maximum water mass loss (19 cm month^{-1} in November) near Kyushu Island.

The climatological monthly surface fresh water flux components for the five sub-areas show similar features: (1) fresh water gain during the summer monsoon season and fresh water loss during the winter monsoon season, and (2) net annual fresh water loss (1.8–4 cm month^{-1}) from the air-ocean interface. Such a long term surface saline process might be compensated for by the river run-off. The seasonal cycle of surface fresh water budget (Fig. 7) shows that E exceeds P during the winter monsoon period (September to March) and P exceeds E during the summer monsoon period (May to August). The shallow water region (YC, ECS, CB) leads the relatively deep region (KC, TWC) by nearly one month to get fresh water. F peaks in July in the YS sub-area and in June else-

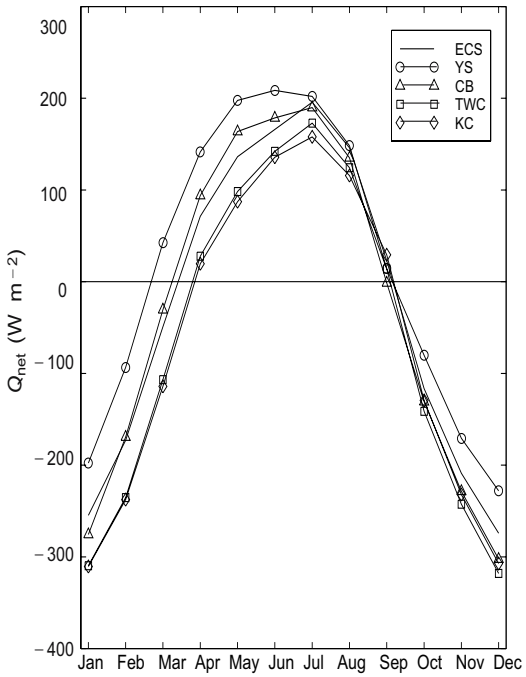

Fig. 5. Seasonal variations of monthly mean net heat flux (W m^{-2}) for the five sub-regions.

where.

3.3.3 *Surface buoyancy flux*

Both $Q_{\rm net}$ and F are in-phase during the seasonal variation: positive (negative) values during the summer (winter) monsoon season. Thus, the surface buoyancy flux,

$$B = \frac{\alpha g Q_{\rm net}}{\rho_{\rm w} c_{\rm pw}} + \beta g (P - E) S_0 \qquad (3)$$

should have a similar seasonal variation as $Q_{\rm net}$ and F. Here, g is gravitational acceleration, $\rho_{\rm w}$ the characteristic water density, $c_{\rm pw}$ the water specific heat under constant pressure, α the water thermal expansion coefficient, β the salinity contraction coefficient, and S_0 the surface salinity. The surface buoyancy flux, B, for the five sub-regions has a similar quasi-sinusoidal seasonal variation with the maximum buoyancy gain (loss) in the summer (winter), which results in a shallow (deep) mixed layer in summer (winter).

4. Hydrographic dataset

The MOODS is a compilation of observed ocean data worldwide consisting of (1) temperature-only profiles; (2) both temperature and salinity profiles, (3) sound-speed profiles, and (4) surface temperatures from drifting buoys. These measurements are, in general, irregular in time and space. In this study, we analyze temperature and salinity profiles measured from a variety of instruments. Due to the shear size (more than six million profiles) and enormous influx of data to the Naval Oceanographic Office from various sources, quality control is a difficult task (Chu et al., 1997c). Our study domain lies inside the area 24°N to 40°N and 118°E to 132°E (Fig. 8); the dataset within this region consisted of nearly 24 000 profiles after rejecting certain data during quality control. These primary editing procedures included removal of profiles with obviously erroneous location, profiles with large spikes, and profiles displaying features that do not match the characteristics of surrounding profiles. In shallow water, this procedure can be partially automated but also involves subjective interpretation because of the under-sampling of MOODS compared to the spatial and temporal variability of the water masses (Chu et al., 1997a, b).

The main limitation of the MOODS data is its irregular distribution in time and space. Certain periods and areas are over sampled while others lack enough observations to provide meaningful insights. Vertical resolution and data quality are also highly variable depending much on instrument type and sampling expertise. A prominent data sparse area is located off the eastern coastal region of China (Fig. 8). The period of 1975 to 1986 is found to have a relatively large number of profiles. Yearly temperature (salinity) casts above 2 000 (400) are 1975, 1976, 1978, 1981, and 1986 (Figs. 9a, b). Within a given year, temporally uneven distributions can be seen such as in the 1984 temperature casts (Fig. 9c) and salinity casts (Fig. 9d). Spatial and temporal irregularities along with the lack of data in certain regions must be carefully weighed in order to avoid statistically-induced variability (Chu et al, 1997c).

5. Seasonal variation of water mass characteristics

5.1 *Relative heat storage*

If we are not interested in the actual heat storage values, but rather in its annual cycle, the relative heat storage (RHS) is useful to arrange our hydrographic dataset on a seasonal basis. The definition of RHS is taken from Hecht et al. (1985),

$$S_{\rm RH} = \begin{cases} \dfrac{D}{H} \displaystyle\int_{-H}^{0} c_p \rho_{\rm w} (T - T_0) dz \,, & \text{if } H < D \\ \displaystyle\int_{-H}^{0} c_p \rho_{\rm w} (T - T_0) dz \,, & \text{if } H \geqslant D \end{cases} \qquad (4)$$

where H is the actual water column depth, D the maximum water depth considered, T the water temperature, and T_0 an arbitrary reference temperature. In our computations, $D = 50$ m, and $T_0 = 5$°C.

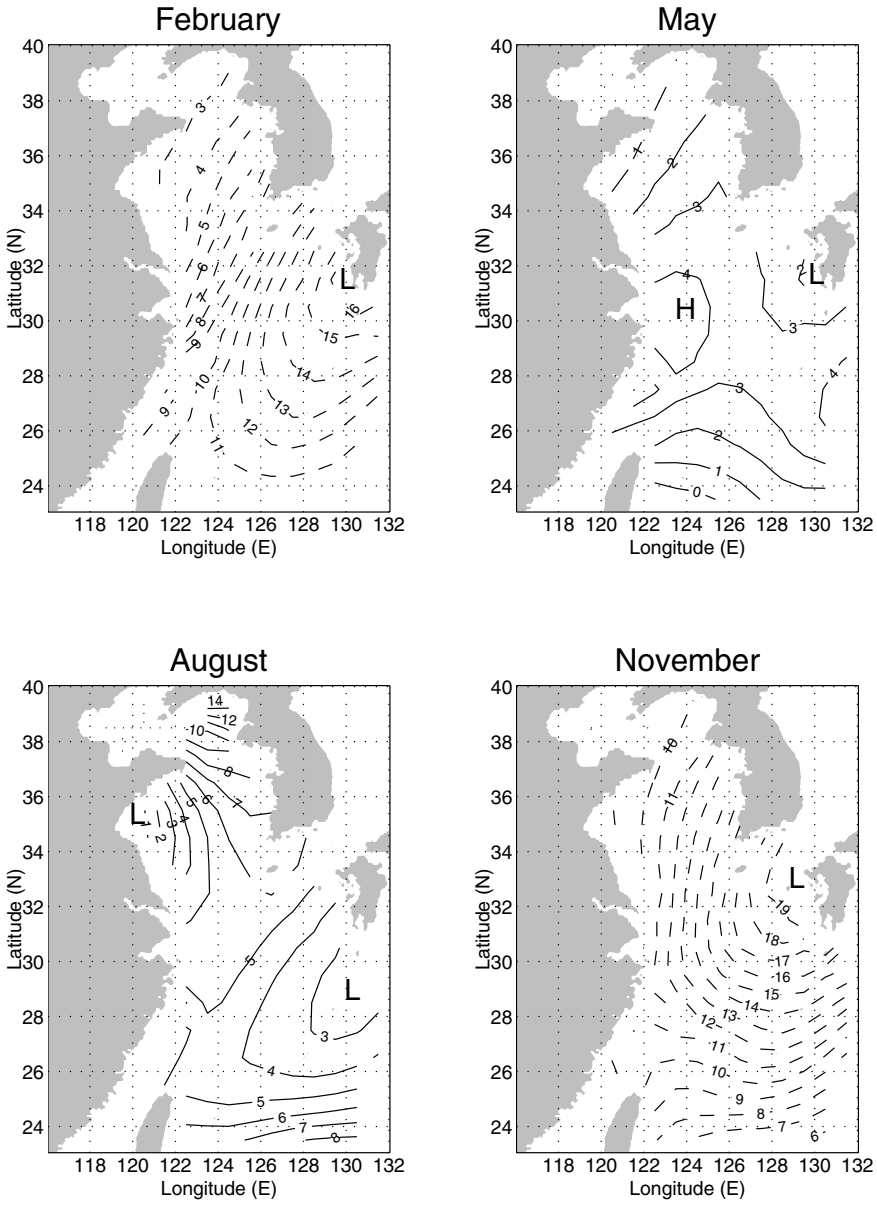

Fig. 6. Average surface fresh water flux (cm month^{-1}) for February, May, August, and November from COADS. Solid (dashed) curves indicate positive (negative) values.

The RHS values for the five sub-areas are shown in Fig. 10. Two extreme seasons can be clearly identified, namely, winter from January to April, and summer from July to November. We can also define the two transition seasons: spring, consisting of May and June, and fall, consisting of December.

5.2 *Temperature and salinity*

In the ECS shelf region, the entire water column exhibits an evident seasonal thermal cycle (Fig. 11a). A well developed thermocline is present down to 30-m depth in spring and extends to the bottom in summer. A significant cooling begins at the end of summer with weakening strength with depth. The whole water column becomes well mixed with temperature near 18°C in autumn. This is probably due to the entrainment mixing generated by strong surface winds, tidal mixing, as well as strong surface buoyancy loss caused by the net heat loss of 274 W m^{-2} (Table 1) and fresh water loss of 13.3 cm month^{-1} (Fig. 7). From autumn to winter, the whole water column is uniformly cooled to 13°C. Total seasonal variability at the bottom is around 6.5°C. The surface salinity S exhibits a minim-

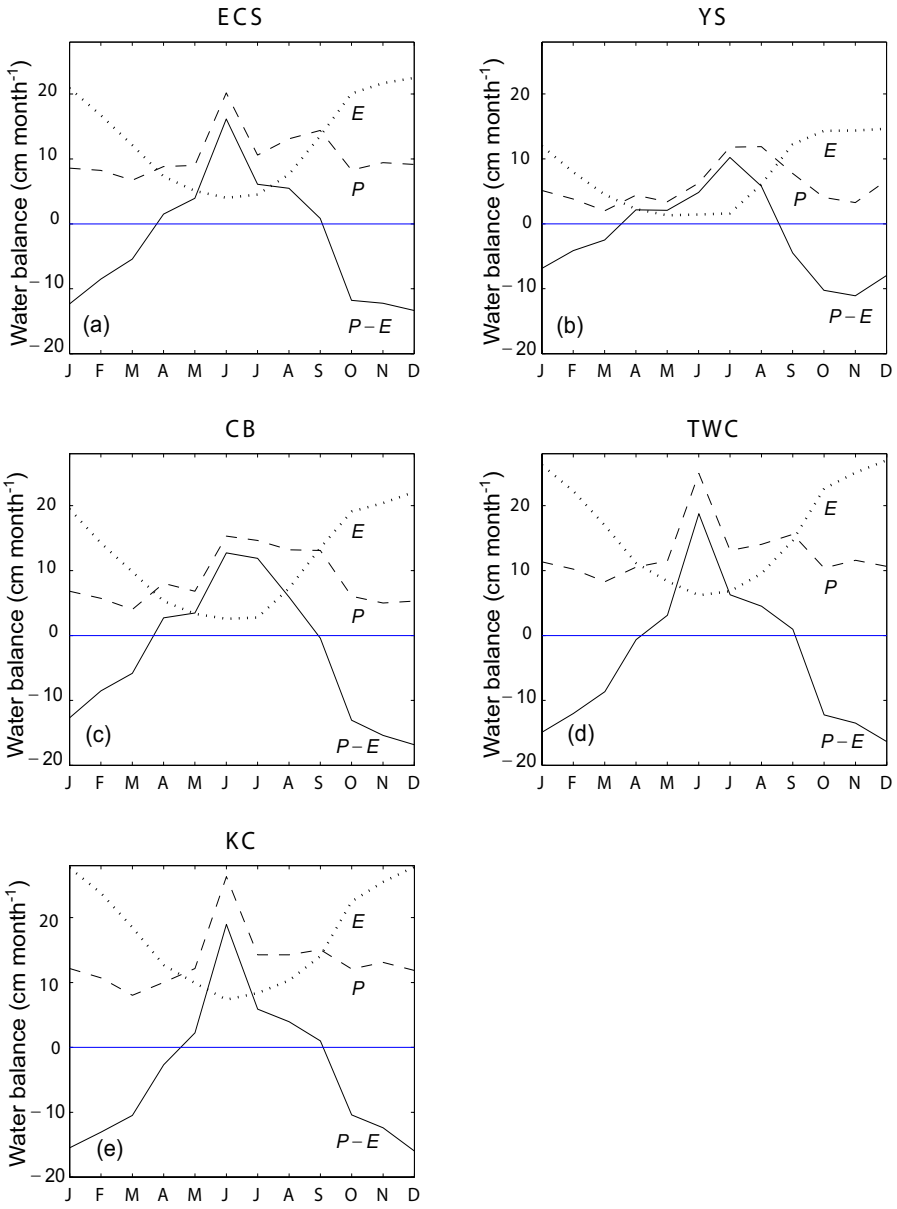

Fig. 7. Seasonal variations of monthly mean fresh water flux (cm month^{-1}) for the five sub-regions.

um value of 32.88 ppt in spring, increases to 33.39 ppt in summer and further increases to its maximum value of 34.08 ppt in autumn, and then decreases to 33.74 ppt in winter (Fig. 12a). From the T-S diagram (Fig. 13a) we can clearly recognize a seasonal layer of the East China Sea Surface Water (ECSSW), which corresponds to relatively low salinities and high temperatures of summer, and an ECSDW layer, which is cooled and renewed in winter. From our data, the ECSDW (open circles in Fig. 13a) has average characteristics of $T = 12.82°C$, $S = 33.88$ ppt, $\sigma_t > 25.2$ kg m^{-3}, which is consistent with an earlier study by Liu et al. (1992). The surface freshness is in-phase with the surface fresh water flux F (Fig. 7a) in such a way that the maximum (minimum) F and the lowest (highest) surface salinity occurs in the same season, spring (autumn). However, the surface dilution is out of phase with the Yangtze River water discharge. The lowest surface salinity (spring) does not occur at the same time as the maximum Yangtze River discharge. This may confirm an earlier study by Beardsley et al. (1985) that the summer fresh water discharge from the Yangtze River forms a relatively shallow, low salinity plume-like structure extending offshore on average to-

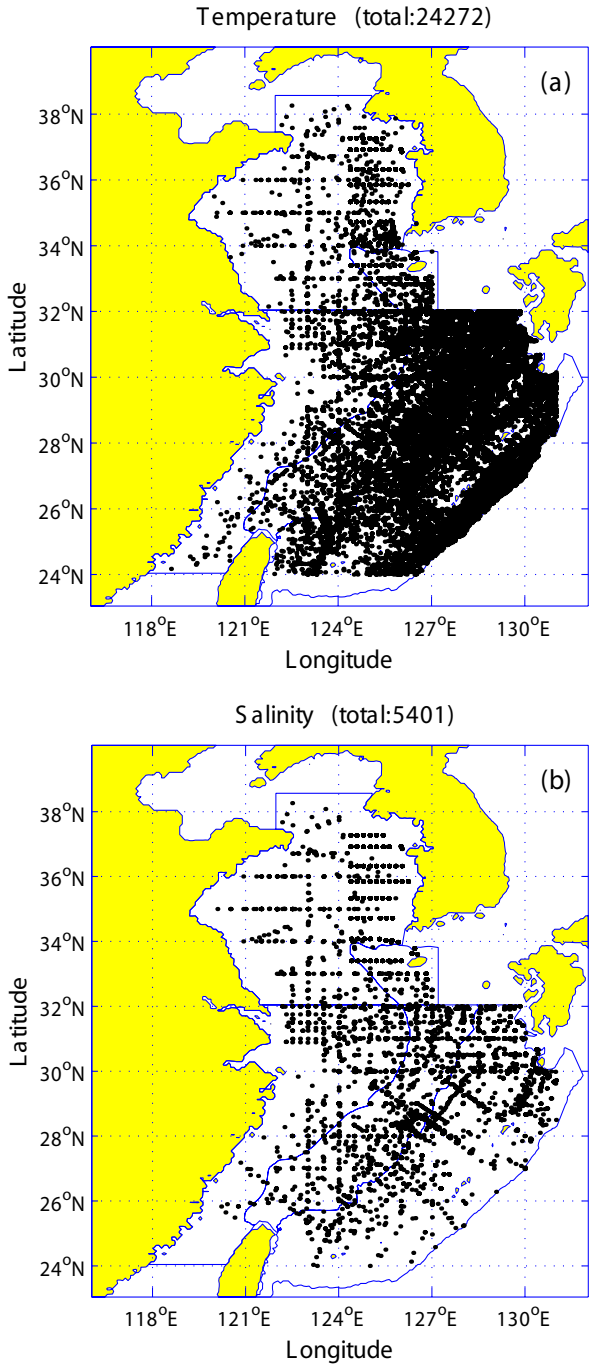

Fig. 8. Spatial distribution of MOODS data during 1975–1986.

wards the northeast. Thus, the dominant factor in determining near-surface salinity is the surface fresh water flux. Besides, a well developed halocline extends to 40-m in spring and summer, being stronger in spring.

In the YS basin, the spring-summer thermocline is formed down to the bottom. The bottom water(Figs. 11b and 12b) is observed as low temperature and moderately-high salinity water with a weak seasonal variation. The winter density, σ_t, is greater than 25.6 kg m^{-3}. These values are consistent with many earlier studies (Lie, 1985, 1987; Li and Yuan, 1992; Chen et al., 1994) describing the characteristics of YSCW near the bottom all year round. The lack of seasonality might be due to the semi-enclosed basin and the bowl-type bottom topography (Fig. 1) which limits mixing with the surrounding waters. The surface waters are freshest in summer ($S = 31.42$ ppt) but rapidly achieve their saltiest condition in autumn (32.98 ppt). The net surface fresh water flux has the maximum value (4.84 cm month^{-1}) in spring, reduces to a value of –1.96 cm month^{-1} (Fig. 7) in summer (July–November) and continues to drop to the minimum value of –7.96 cm month^{-1} (Fig. 7) in autumn. Such a mismatch between surface salinity and F may suggest that the dominant factor for determining the near surface salinity structure in summer is the river run-off. This coincides with Chen et al.'s (1994) results based on hydrographic observations during 1986. From the $T-S$ diagram (Fig. 13b) we can clearly recognize a seasonal variation of the YSCW, which is cooled and renewed in winter. We may define the YSCW having winter characteristics of $T = 6.5$°C, S=32.75 ppt, and $\sigma_t > 25.6$ kg m^{-3}. These values are consistent with an earlier study by Liu et al. 1992.

In the CB region, there is a strong seasonal variation. A spring-summer thermohaline is present but weak (Figs. 11c, 12c). From summer to autumn, a significant cooling takes place close to the surface and weakens with depth. The whole water column becomes well mixed with temperature near 17.0°C in autumn. In winter, the whole water column is uniformly cooled to 14.3°C. Total seasonal thermal variability at the bottom is around 5.0°C. The surface salinity has a minimum value of 31.46 ppt in summer, increases to 33.99 ppt in autumn and further increases to the maximum value of 34.41 ppt in winter, and then decreases to 32.68 ppt in spring (Fig. 12c). Total seasonal haline variability at the bottom is around 1.69 ppt. Beardsley et al. (1985) indicates that the TWC bifurcates near the CB region into the Yellow Sea Warm Current and the Tsushima current. There should be some connection between the CB region and the upper layer (30 m) of the TWC region. However, the similarity between CB and upper TWC profiles only occurs in temperature but not in salinity (Figs. 11c and d). The seasonal surface salinity variation follows the seasonal cycle of F: minimum salinity and maximum surface fresh water flux in summer and the opposite in winter. From the $T-S$ diagram (Fig. 13c) we can clearly recognize the TWC deep water (TWCDW) and YEMW.

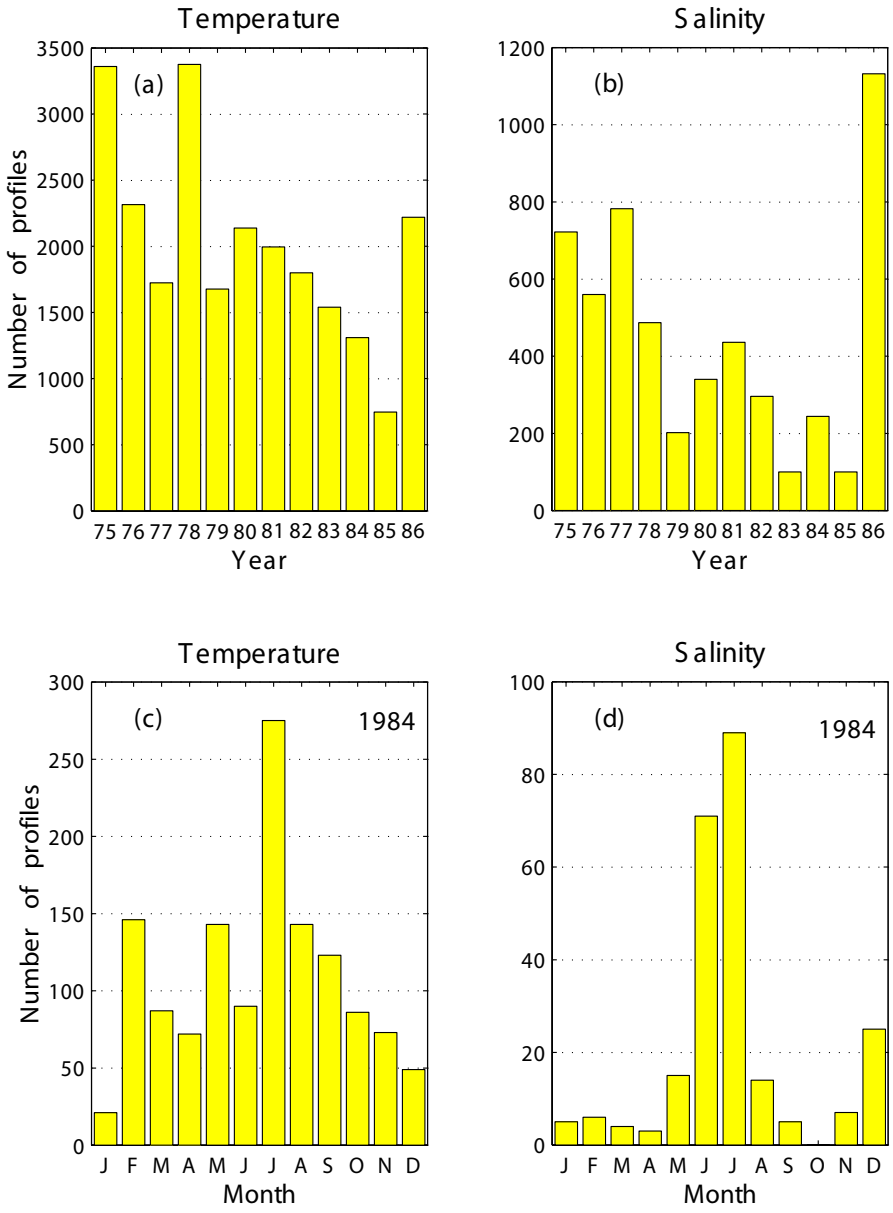

Fig. 9. Temporally irregular cast distribution: (a) yearly temperature, (b) yearly salinity, (c) monthly temperature in 1984, and (d) monthly salinity in 1984.

In the TWC region, the upper water column (surface to 60 m), usually called the TWC Upper Water (TWCUW), exhibits an evident seasonal thermohaline cycle (Figs. 11d, 12d). Total seasonal variability of temperature (salinity) is around 7°C (1.02 ppt) at the surface and weakens with depth. Below 60 m depth, there exists a permanent thermocline with very weak seasonal variation. At the bottom (150 m), the water properties are seasonally invariant; the temperature is about 15°C, and the salinity is around 34.62 ppt. In winter, the surface waters are cool with a temperature of 19°C. Significant warming begins in spring with a 4.0°C increase from winter conditions followed by a 3°C increase from spring to summer. In summer, the surface temperature reaches its maximum of 26.3°C. Significant cooling (4.7°C) occurs in autumn. The surface salinity has the minimum value of 33.67 ppt in summer, increases to the maximum value of 34.69 ppt in autumn and slightly decreases to 34.52 ppt in winter, and then decreases to 33.91 ppt in spring. The surface freshness is in-phase with the surface fresh water flux F (Fig. 7d). From the $T-S$ diagram (Fig. 13d) we can clearly recognize a seasonal layer of TWC, which is relatively fresh and warm in summer and saline and

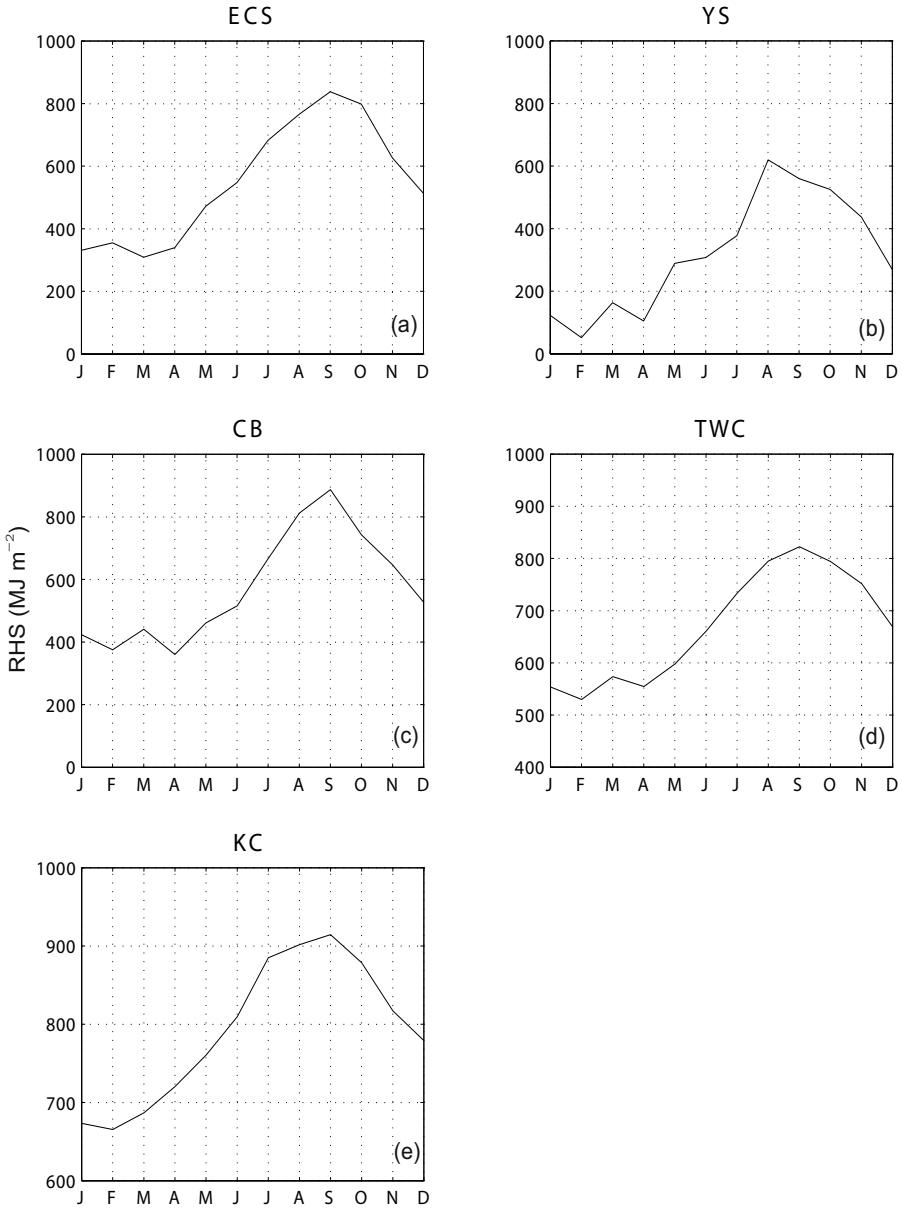

Fig. 10. Seasonal variations of monthly mean relative heat storage for the five subregions.

cool in winter.

In the KC region the upper water column (surface to 80 m), usually called the Kuroshio Surface Water (KSW), exhibits an evident seasonal thermal cycle (Figs. 11e, f; 12e, f). Total seasonal variability of temperature (salinity) is around 5.7°C (0.47 ppt) at the surface and weakens with depth. From 80 to 600 m, there exists a permanent thermocline/halocline with very weak seasonal variation. At 1500 m depth, the temperature is about 3.7°C and the salinity is around 34.43 ppt. In winter, the surface has a minimum temperature (21.7°C). A significant warming begins in spring. There is a 3.7°C increase from winter to spring and a 2.0°C increase from spring to summer. In summer, the surface temperature reaches its maximum (27.4°C). A significant cooling starts in autumn. There is a 3.7°C decrease from summer to autumn. The surface salinity has the minimum value of 34.29 ppt in summer, increases to the maximum value of 34.75 ppt in winter, and then decreases to 34.56 ppt in spring. The surface freshness is in-phase with the surface fresh water flux F (Fig. 7d). Our data also show the existence of S-type salinity profiles with a maximum salinity in the layer between 150 and 250 m, which

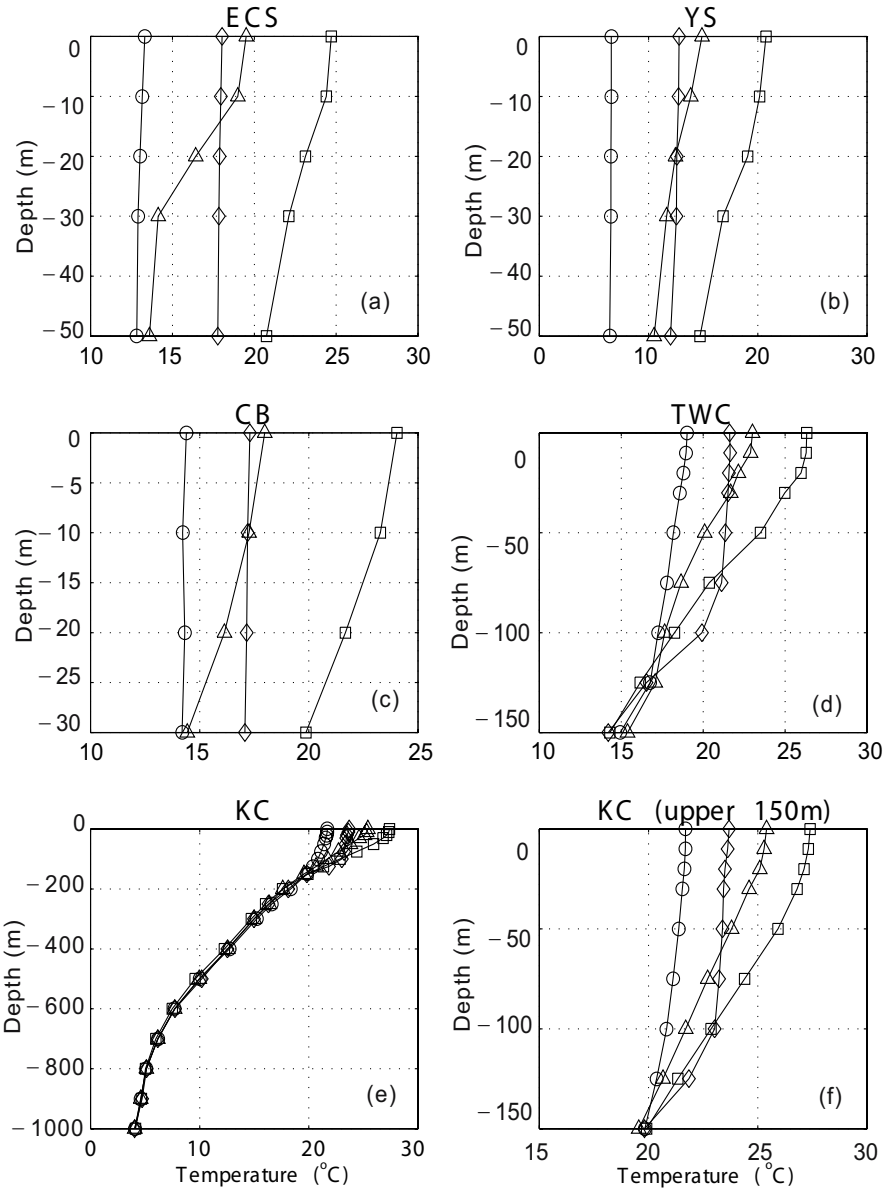

Fig. 11. Seasonal climatological profiles of temperature for the five sub-regions: (a) the ECS shelf, (b) YS, (c) CB, (d) TWC, (e) KC regions, and (f) upper (0–150 m) KC regions. The symbol "o" denotes winter, "Δ" denotes spring, "□" denotes summer and "◊" denotes fall.

is associated with the Kuroshio Sub-Surface Water (KSSW); and with a minimum salinity at 600 m depth, which is associated with the Kuroshio Intermediate Water (KIW). In the sublayer between 150 m and 450 m, the salinity decreases with depth. From the $T-S$ diagram (Figs. 13e, f) we can clearly recognize a seasonal layer of KC, which is relatively fresh and warm in summer and saline and cool in winter. Putting five $T-S$ diagrams (Figs. 13a–e) into one $T-S$ diagram, the five sub-regions and various ECS/YS water masses are well represented (Fig. 14). We can see the connections and mixing of water masses among the five sub-regions. For example, the water masses in the CB region come from TWCDW, YEMW, and YSMW. The YS and ECS waters are mixed during spring and summer. Besides, various ECS/YS water masses are well classified on this $T-S$ diagram.

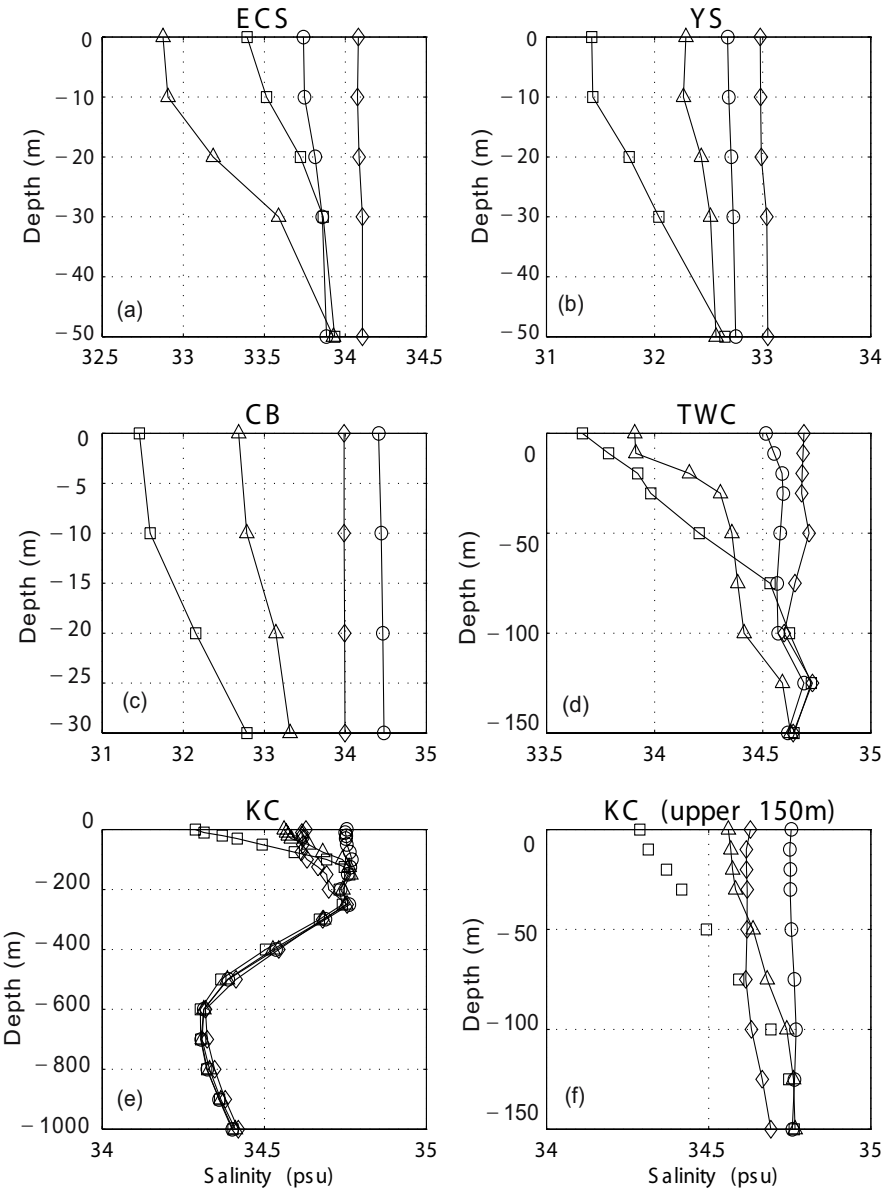

Fig. 12. Same as Figure 11 except for salinity.

7. Conclusions

The work presented here describes seasonal variability of water mass structure of the East China Sea and Yellow Sea. Based on the current system and bathymetry, we divided the area into five sub-regions: the East China Sea shelf, the Yellow Sea basin, the Cheju bifurcation zone, the Taiwan Warm Current area, and the Kuroshio Current area. We use the U.S. Navy's Master Oceanographic Observation Data Set and the Comprehensive Ocean-Atmosphere Data Set to investigate the linkage between the fluxes (momentum, heat, and moisture) across the air-ocean interface and the formation of the water mass features for the five sub-regions.

(1) The most important atmospheric forcing is the strong winter monsoon (north to northeast) and weak summer monsoon (southeast). The surface air temperature has a nearly latitudinal gradient with a south-to-north difference of 18°C in February and 3°C in August. The surface relative humidity is generally higher in the summer season, mainly as a consequence of the southeast summer monsoon bringing moist air from the Tropics. A relative humidity minimum (maximum) is present in all seasons near Kyushu Island

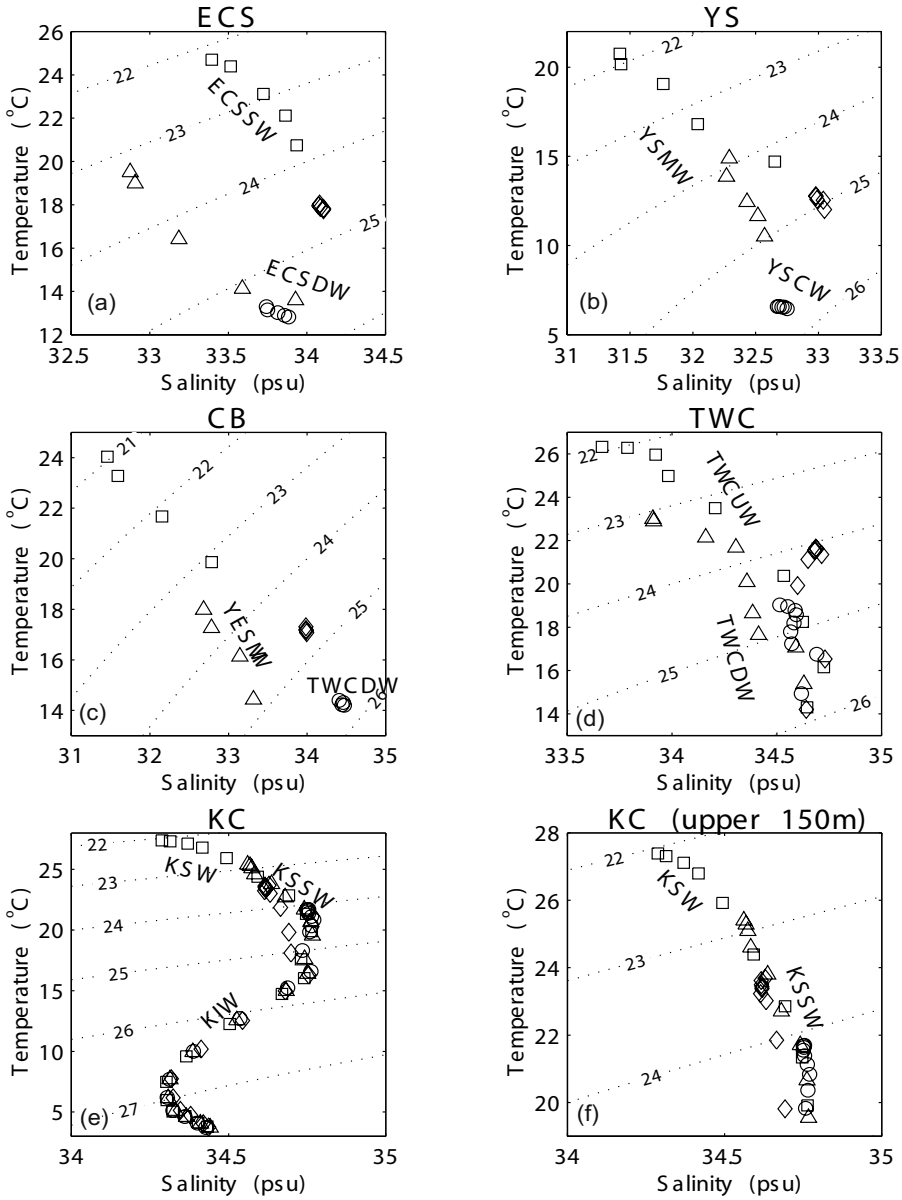

Fig. 13. Seasonal climatological T–S diagrams for the five sub-regions: (a) the ECS shelf, (b) YS, (c) CB, (d) TWC, (e) KC regions, and (f) upper (0–150 m) KC regions. The symbol "o" denotes winter, "Δ" denotes spring, "□" denotes summer and "◇" denotes fall.

(Chinese coast), which may lead to maximum (minimum) evaporation there.

(2) The air-sea heat budget at the surface is dominated by the incoming solar radiation balanced by latent and longwave heat energy loss. It was found that the Yellow Sea has an overall long term heat gain of 15 W m^{-2} (caused by low latent heat flux), and the rest of the area has an overall heat loss of around 30 W m^{-2} in the East China Sea and Cheju bifurcation zone, and of 65 W m^{-2} in the Kuroshio and Taiwan Warm Current regions. The sensible heat flux is nearly zero in summer, which implies SST is close to SAT. The monthly variation of net surface heat flux is nearly sinusoidal and quite similar among the five sub-areas. $Q_{\rm net}$ peaks in June in the Yellow Sea and in July in the rest of the sub-areas.

(3) The air-sea fresh water budget exhibits a distinct winter fresh water loss and summer fresh water gain pattern. The whole area experiences an overall fresh water loss (1.8–4 cm month^{-1}) at the surface.

(4) The East China and Yellow Seas do not follow the usual atmospheric seasons. We divided the four

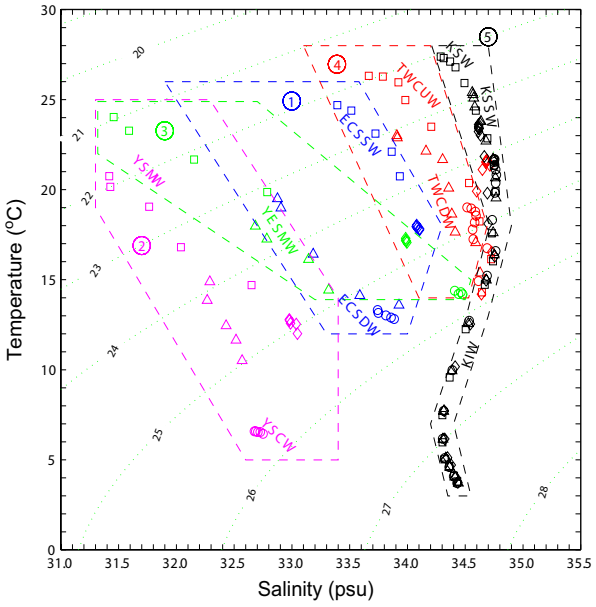

Fig. 14. Water mass classification on the climatological $T - S$ diagram.

seasons based on the relative heat storage, namely, winter (January–April), spring (May–June), summer (July–November), and autumn (December).

(5) We have classified the water masses of the East China and Yellow Seas using climatological averages. The entire water column of the East China Sea shelf water and the Yellow Sea (including the Cheju bifurcation zone) undergoes an evident seasonal thermal cycle with maximum values of temperature during summer and maximum mixed layer depths during winter. However, only the surface waters of the Taiwan Warm Current region (upper 60 m) and the Kuroshio region (upper 80 m) exhibit a seasonal thermal cycle. Below these depths, there is no evident seasonal variation.

(6) The salt balance of the surface layer is clearly affected by surface fresh water flux and river runoff. In the East China Sea shelf region, the surface freshness (low salinity) is in-phase with the surface fresh water flux ($P - E$) and out-of-phase with the Yangtze River water discharge. The lowest surface salinity (spring) does not occur at the same time as the maximum Yangtze River discharge (July). In the Yellow Sea, however, the surface freshness is out-of-phase with the surface fresh water flux and in-phase with the Yangtze River water discharge. Two different relations between surface salinity and Yangtze River runoff, out-of-phase in the East China Sea shelf and in-phase in the Yellow Sea, may confirm an earlier study by Beardsley et al. (1985) showing that the summer fresh water discharge from the Yangtze River forms a relatively shallow, low salinity plume-like structure extending offshore on average towards the northeast.

Acknowledgments. The authors are grateful to C. W. Fan at the Naval Postgraduate School for his programming assistance. This work was funded by the Naval Oceanographic Office, the Office of Naval Research NOMP Program, and the Naval Postgraduate School.

REFERENCES

Beardsley, R. C., R. Limeburner, H. Yu, and G. A. Cannon, 1985: Discharge of the Changjiang (Yangtze River) into the East China Sea. *Continental Shelf Research*, **4**, 57–765.

Chen, C. S., R. C. Beardsley, R. Limeburner, and K. Kim, 1994: Comparison of winter and summer hydrographic observations in the Yellow and East China Seas and adjacent Kuroshio during 1986. *Continental Shelf Research*, **14**, 909–929.

Chu, P. C., C. R. Fralick, S. D. Haeger, and M. J. Carron, 1997a: A parametric model for Yellow Sea thermal variability. *J. Geophys. Res.*, **102**, 10499–10508.

Chu, P. C., S. K. Wells, S. D. Haeger, and M. J. Carron, 1997b: Spatial and temporal scales of the Yellow Sea thermal variability. *J. Geophys. Res.*, **102**, 5655–5668.

Chu, P. C., H. C. Tseng, C. P. Chang, and J. M. Chen, 1997c: South China Sea warm pool detected in spring from the Navy's Master Oceanographic Observational Data Set (MOODS). *J. Geophys. Res.*, **102**, 15761–15771.

Chu, P. C., Y. C. Chen, and S. H. Lu, 1998: On Haney-type surface thermal boundary conditions for ocean circulation models. *Journal of Physical Oceanography*, **28**, 890–901.

Chu, P. C., S. H. Lu, and C. W. Fan, 2001: An air-ocean coupled nowcast/forecast system for the East Asian marginal seas. *Advances in Mathematical Modeling of Atmosphere and Ocean Dynamics*, Kluwer Scientific Publishing Co., 137–142.

Haney, H. L., 1971: Surface thermal boundary condition for ocean circulation model. *Journal of Physical Oceanography.*, **1**, 241–248.

Hirose, N., H.-C. Lee, and J.-H. Yoon, 1999: Surface heat flux in the East China Sea and Yellow Sea. *Journal of Physical Oceanography.*, **29**, 401–417.

Li, H., and Y. Yuan, 1992: On the formation and maintenance mechanisms of the cold water mass of the Yellow Sea. *Chinese Journal of Oceanology and Limonology*, **10**(2), 97–106.

Lie, H.-J., 1985: Wintertime temperature-salinity characteristics in the Southeastern Hwanghae (Yellow Sea). *Journal of Oceanographic Society of Japan*, **41**, 291–298.

Lie, H.-J., 1987: Summertime hydrographic features in the Southeastern Hwanghae (Yellow Sea). *Progress in Oceanogrophy*, **17**, 229–242.

Liu, S., X. Shen, Y. Wang, and S. Han, 1992: Preliminary analysis of distribution and variation of perennial monthly mean water masses in the Bohai Sea, the

Huanghai (Yellow) Sea and the East China Sea. *Acta Ocearologica Sinica*, **11**, 483–498.

Su, Y.-S., and X.-C. Weng, 1994: *Water masses in China Seas.* Vol. 1, *Oceanology of China Seas*, Zhou Di et al., Eds., Kluwer Academic Publishers, Boston, 3–16.

Takahashi, S., and T. Yanagi, 1995: A numerical study on the formation of circulations in the Yellow Sea during summer. *La mer*, **33**, 135–147.

Tomczack, M., and J. S. Godfrey, 1994: *Regional Oceanography: An Introduction.* Daya Publishing House, Delhi, India, 516pp.

van Loon, H., 1984: *Climates of the Oceans. World Survey of Climatology*, **15**, 453–458.

Watts, I. E. M., 1969: Climates of China and Korea. *World Survey of Climatology*, **8**, 1–117.

Yanagi, T., and S. Takahashi, 1993: Seasonal variation of circulations in the East China Sea and the Yellow Sea. *J. Oceanogr.*, **49**, 503–520.